Robust Machine Tool Thermal Error Modeling Through Thermal Mode Concept

Jie Zhu

Jun Ni

Albert J. Shih

Department of Mechanical Engineering,
University of Michigan,
Ann Arbor, MI 48109

Thermal errors are among the most significant contributors to machine tool errors. Successful reduction in thermal errors has been realized through thermal error compensation techniques in the past few decades. The effectiveness of thermal error models directly determines the compensation results. Most of the current thermal error modeling methods are empirical and highly rely on the collected data under specific working conditions, neglecting the insight into the underlying mechanisms that result in thermal deformations. In this paper, an innovative temperature sensor placement scheme and thermal error modeling strategy are proposed based on the thermal mode concept. The modeling procedures for both position independent and position dependent thermal errors are illustrated through numerical simulation and experiments. Satisfactory results have been achieved in terms of model accuracy and robustness.
[DOI: 10.1115/1.2976148]

Introduction

The importance of enhancing machine tool accuracy has been well recognized in both industry and academia in the past few decades, largely due to the increasing demands for products with better quality and tighter tolerances while still maintaining high productivity. The machine tool accuracy directly determines the dimensional accuracy of machined products. The most significant factor influencing the machine tool accuracy is the thermal error, which accounts for 40–70% of total machine tool errors [1]. Internal and external heat sources can cause thermal deformations in machine tool structures far beyond the acceptable dimensional tolerances of common machined products.

Researchers have been investigating the influences of thermal errors on the machine tool accuracy and seeking solutions to reduce these errors for decades. Examples of successful thermal error reduction with the aid of error compensation techniques have been demonstrated in both research laboratories and industrial facilities [2–6]. However, the accuracy and robustness of the thermal error models are still considered as the major barriers preventing widespread application of thermal error compensation [7].

Some researchers concentrated on the development of thermal error models by using various modeling methodologies. These methods include polynomial regression [2,4], artificial neural networks [8–11], and system identification [12–14]. The locations of the temperature sensors are generally selected to be as close as possible to heat sources in most researches. Consequently, either the deficient number or the improper locations of the temperature sensors undermines the effectiveness of the thermal error models. To resolve this problem, statistical methods are employed to choose temperature sensors at certain key positions from an excessive number of sensors mounted on the machine according to the ranked contributions to a specified measure [15–17]. In general, an extensive amount of time and effort is required for the machine characterization, variable selection, and model training to develop a machine tool thermal error model [7].

The abovementioned methods are mostly empirical, and the thermal error models thus derived are sensitive to the specific model training conditions of each study. One of the main reasons is that the essence of the underlying thermal deformation process has been neglected. Very limited research has been done to reveal the importance of thermo-elastic relationship in machine tools. Lo [18] illustrated the hysteresis effect between temperature and deformation of a simplified spindle model. Ma et al. [19] provided an analytical description and pointed out the dependence of temperature sensor locations on the frequency of heat inputs due to the effects such as machining cycles and daily shifts.

Ma [20] proposed a thermal deformation modal analysis to further explore the thermo-elastic relationship using the finite element analysis (FEA). However, Ma was not able to develop experimental methods to realize the thermal deformation modal analysis. Similar to the dynamic modal analysis, a small number of significant modes are supposed to dominate the entire thermal deformation process. If temperature sensors are mounted on certain locations to capture these dominant modes, more accurate and robust thermal error models would be developed correspondingly. Many schemes already exist for optimal sensor placement to analyze dynamic systems, including covariance matrix [21], eigensystem realization [22], modal kinetic energy [23], and effective independence [24] approaches. Those schemes could be modified to resolve the conceptually similar thermal deformation problems.

In this paper, a new temperature sensor placement strategy is presented based on the thermal modal analysis. The purpose of this strategy is to acquire the dominant thermal modes in the thermal deformation process. The linear independence between collected temperature data sets is thus increased to enhance the thermal error model estimation accuracy. In addition, the existence of thermal modes is practically unveiled in machine tool elements. The effectiveness of the derived thermal error models based on this proposed approach will be verified through both simulation and experiments.

The rest of this paper will be arranged as follows. In Sec. 2, the thermal modal analysis is first introduced. The temperature sensor placement and thermal error modeling based on the thermal mode concept will be discussed in Sec. 3. The validity of this approach will be demonstrated through numerical simulation in Sec. 4 and experiments in Sec. 5.

2 Thermal Modal Analysis

2.1 Thermal Modes. FEA has been exploited by some researchers investigating the machine tool thermal errors in order to

Contributed by the Manufacturing Engineering Division of ASME for publication in the JOURNAL OF MANUFACTURING SCIENCE AND ENGINEERING. Manuscript received February 20, 2008; final manuscript received May 25, 2008; published online October 10, 2008. Review conducted by Dong-Woo Cho.

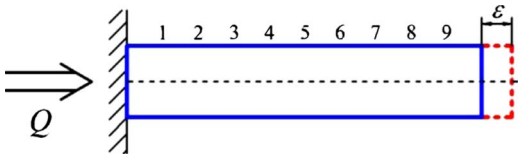

Fig. 1 Simplified spindle model

consolidate the conventionally empirical approaches [25–28]. Finite element modal analysis is also used to resolve dynamics [21–24] and heat transfer problems [29,30]. However, finite element modal analysis is seldom utilized to explore the essence of machine tool thermo-elastic problems, even though the similar idea of decomposing a complicated system into simpler subsystems without the loss of substantial characterization has been proposed. Matsuo et al. [31] evaluated the steady-state temperature and the rate of temperature rise of a machine tool structure to shorten the machine warm-up period based on the modal analysis. Weck et al. [32] expressed the measured thermal errors in response to a steplike thermal load as a sum of two exponential functions, which were named modes. Ahn and Chung [33] designed an observer to estimate the temperature distribution and expansion of a ball screw system based on the modal analysis of one-dimensional heat transfer problem.

To perform the thermal modal analysis, the finite element solution of the underlying heat transfer problem needs to be solved, which requires the integration of coupled differential equations of the form

$$[C_T]\{\dot{T}(t)\} + [K_T]\{T(t)\} = \{Q(t)\} \tag{1}$$

where $[C_T]$ is the heat capacity matrix, $[K_T]$ is the heat conductivity matrix, $\{T(t)\}$ is the nodal temperature vector, and $\{Q(t)\}$ is the nodal thermal load vector.

The eigen-problem [20] associated with Eq. (1) is

Table 1 Geometric parameters and material properties of the spindle

Material properties		Value	Unit
Heat conduction coefficient	k	60.5	W/m K
Heat capacity	c	434	J/kg K
Density	ρ	7.8×10^3	kg/m^3
Heat convection coefficient	h	20	W/m^2 K
Thermal expansion coefficient	α	10.8	μm/m K
Young's modulus	E	120	GPa
Poisson's ratio	ν	0.25	
Length	L	1.0	m
Area	A	0.0314	m^2

$$[K_T][\Phi_T] = [C_T][\Phi_T][\Lambda] \tag{2}$$

where $[\Lambda]$ is a diagonal matrix composed of all the eigenvalues, λ_i, and $[\Phi_T]$ is the corresponding eigenvector matrix. Theoretically, λ_i is the reciprocal of the corresponding time constant

$$\lambda_i = \frac{1}{\tau_i} \tag{3}$$

where λ_i and τ_i are the ith eigenvalue and time constant, respectively. The time constant describes how quickly the mode responds to thermal loads.

Similar to the dynamic modal analysis, each mode includes one eigenvalue and eigenvector. The smallest eigenvalue, or the largest time constant, corresponds to the lowest mode. The thermal modes, including time constants and the corresponding temperature fields, are the intrinsic properties of a machine tool structure and its working conditions. They are independent of the magnitudes or the locations of thermal loads.

In the modal analysis, the eigenvector matrix $[\Phi_T]$ is used as a

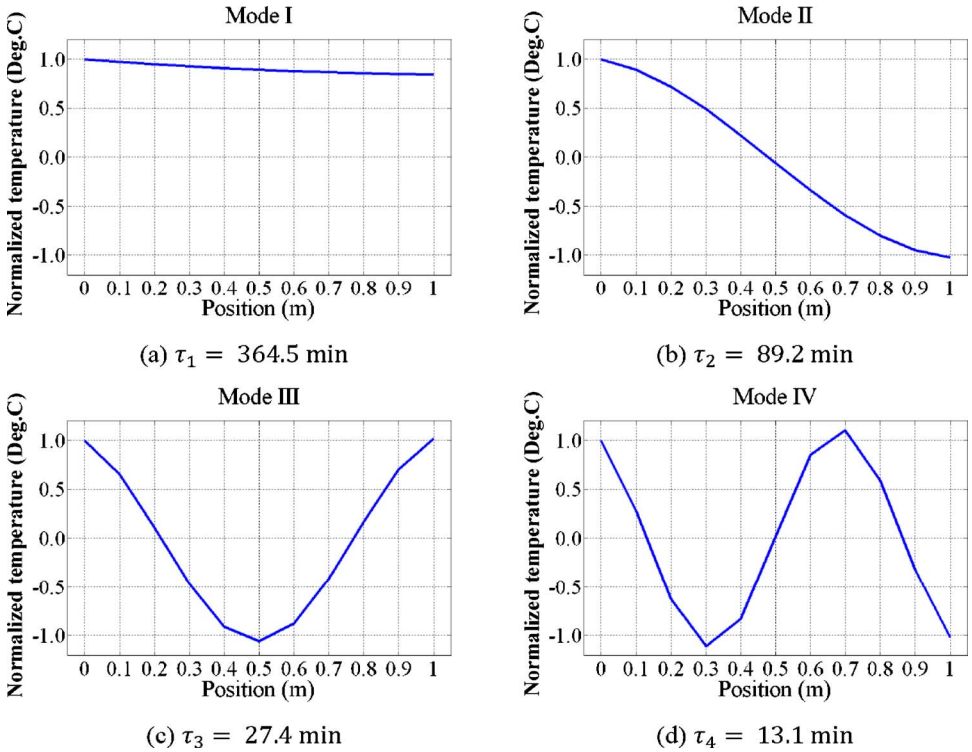

(a) $\tau_1 = 364.5$ min (b) $\tau_2 = 89.2$ min

(c) $\tau_3 = 27.4$ min (d) $\tau_4 = 13.1$ min

Fig. 2 First four thermal modes with temperature fields and time constants: (*a*) mode I, (*b*) mode II, (*c*) mode III, and (*d*) mode IV

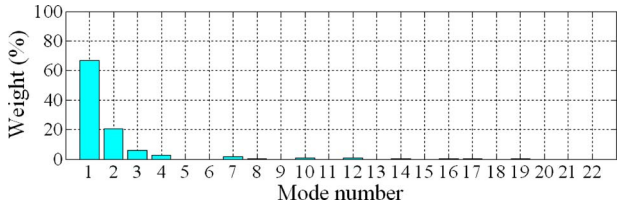

Fig. 3 Weight distribution of thermal modes

transformation matrix to decouple Eq. (1). Nodal temperature $\{T(t)\}$ is then transformed into modal temperature $\{\theta(t)\}$,

$$\{T(t)\} = [\Phi_T]\{\theta(t)\} \tag{4}$$

Substituting Eq. (4) into Eq. (1) and multiplying both sides by $[\Phi_T]^T$,

$$[\Phi_T]^T[C_T][\Phi_T]\{\dot{\theta}(t)\} + [\Phi_T]^T[K_T][\Phi_T]\{\theta(t)\} = [\Phi_T]^T\{Q(t)\} \tag{5}$$

where $[\Phi_T]^T[C_T][\Phi_T]$ is the modal heat capacity matrix, $[\Phi_T]^T[K_T][\Phi_T]$ is the modal heat conductivity matrix, and $[\Phi_T]^T\{Q(t)\}$ is the modal thermal load.

Since the eigenvector is $[C_T]$ orthonormal, the modal heat conductivity and capacity matrices satisfy

$$[\Phi_T]^T[C_T][\Phi_T] = [I] \tag{6}$$

$$[\Phi_T]^T[K_T][\Phi_T] = [\Lambda] \tag{7}$$

Introducing Eqs. (6) and (7) into Eq. (5)

$$\{\dot{\theta}(t)\} + [\Lambda]\{\theta(t)\} = [\Phi_T]^T\{Q(t)\} = \{\xi(t)\} \tag{8}$$

where $\{\xi(t)\}$ is the modal thermal load vector.

Equation (8) is decoupled and can be expressed as a set of single variable, first order differential equations

$$\dot{\theta}_i(t) + \frac{\theta_i(t)}{\tau_i} = \xi_i(t) \tag{9}$$

where $\xi_i(t)$ denotes the modal thermal load. If a step-like heat input is imposed, the solution to Eq. (9) is

$$\theta_i(t) = \xi_i\tau_i(1 - e^{-t/\tau_i}) \tag{10}$$

A step input is widely used for the analysis of linear systems. The thermal load variation of a machine tool can also be approximated as a serial combination of step inputs. The overall temperature response is thus regarded as the superposition of the thermal modes.

In practice, heat capacity matrix, heat conductivity matrix, and nodal thermal load vector are extracted by using MSC/NASTRAN direct matrix abstraction program (DMAP). The time constants and temperature field mode shapes are then obtained by eigen-analysis.

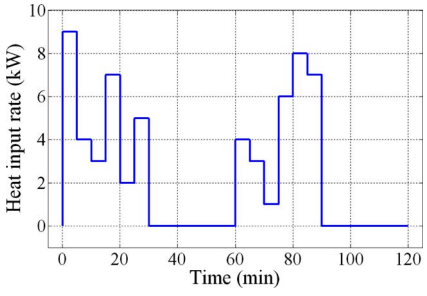

Fig. 4 Heat input for spindle expansion simulation

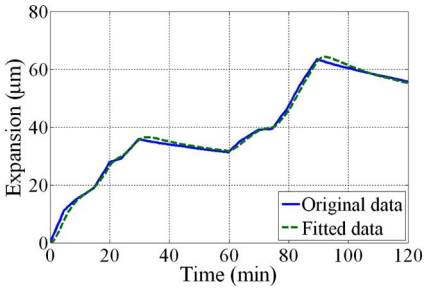

Fig. 5 Simulation and modeling results of the spindle model

2.2 Mode Truncation. One advantage of thermal modal analysis is that the entire thermal deformation process of a machine tool is represented by several dominant thermal modes. To do this, the weight of each mode is defined as

$$w_i = |\xi_i\tau_i| \tag{11}$$

where ξ_i denotes the modal thermal load and τ_i is the time constant of each mode. The magnitude of the weight quantifies the significance of each mode. A small number of modes usually occupy a large percentage of the total weights. The thermal deformation process is then described by these dominant modes. The remaining insignificant modes are discarded.

3 Robust Thermal Error Modeling

Robustness of a thermal error model refers to the applicability of the derived model under different working conditions than model training conditions. Temperature sensor locations play a vital role in determining the robustness of a thermal error model [7].

3.1 Temperature Sensor Placement. Thermal modal analysis provides a systematic method to characterize the thermal behavior of a machine tool by using several dominant modes. To capture these modes, temperature sensors have to be mounted on the machine tool. In simulation, it might be possible to compare the effects of the temperature collected at different locations based on mathematical models. In practice, however, it is time-consuming, and sometimes almost impossible, since some locations may not be accessible, while others might not be appropriate for temperature sensor placement. Moreover, temperature reading is generally not very sensitive to the locations because of the smooth distribution of the temperature field. In other words, temperature sensors within certain area play the similar role, not making much difference in the derivation of thermal error models.

Guidelines are thus desired to efficiently identify the potentially significant sensor locations for developing thermal error models. The guidelines are proposed based on the thermal modal analysis; therefore, it is physically meaningful. Similar to dynamic modal analysis, it is always desirable to place the temperature sensors away from the nodes of the target mode; otherwise no useful

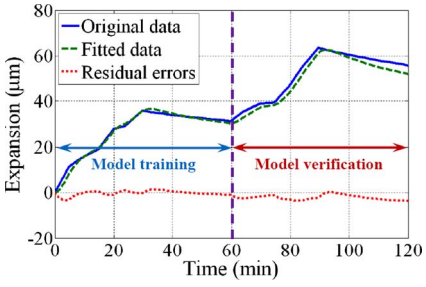

Fig. 6 Linear extrapolation examination of the thermal error model

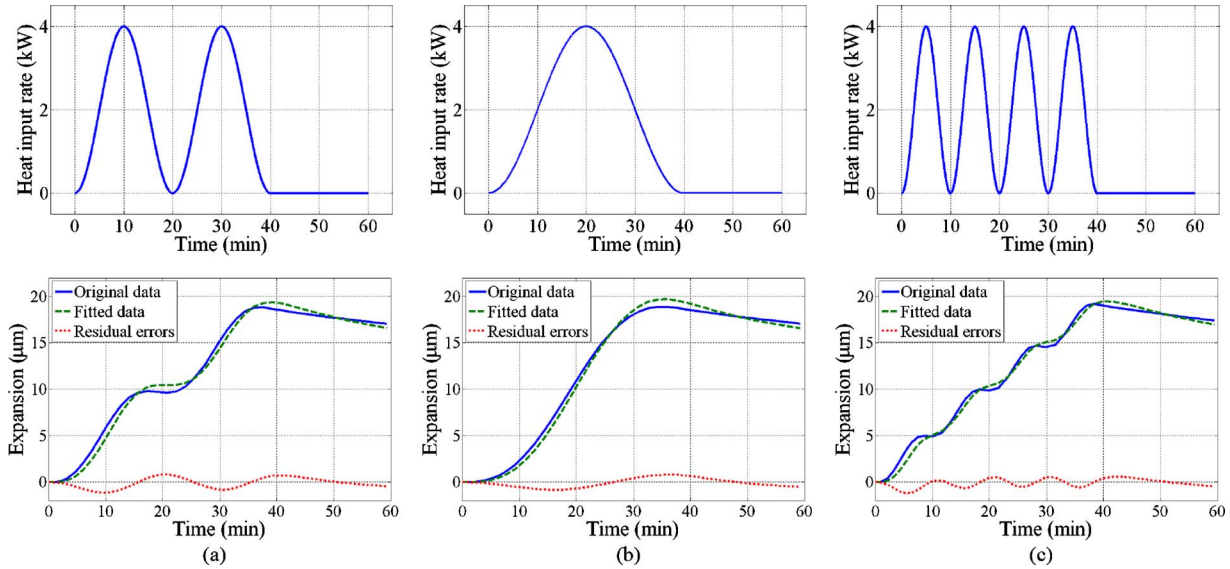

Fig. 7 Frequency sensitivity examination of the thermal error model: (*a*) *T*=20 min, (*b*) *T*=40 min, and (*c*) *T*=10 min

information is collected for that mode. By placing the temperature sensors close to the extreme values of the dominant temperature fields and close to the heat sources, the dominant thermal modes are acquired, the multicollinearity [7] of the collected temperature is reduced, and the signal-to-noise ratio of the collected temperature data is enhanced as well.

Another advantage of this strategy is cost-effectiveness. Once sensors are mounted on the machine tool structure, it is difficult to remove them. The conventional temperature sensor selection method, however, requires a large number of sensors to be mounted in the first place so that the accuracy and robustness of the thermal error models could be improved [19]. The proposed method provides an alternate way to place temperature sensors. Only if the number of sensors is not enough, i.e., the number of representative thermal modes cannot fully describe the thermal deformation process, additional sensors are then mounted to capture more thermal modes. By doing this, the number of temperature sensors is under proper control.

3.2 Thermal Error Modeling. Temperature sensor locations are determined following the guidelines based on the thermal modal analysis. Thermal error models are then derived to relate the temperature collected at these locations to the thermal deformation. Thermal errors of machine tools are generally divided into two categories, position independent and position dependent [4]. Position independent thermal errors, merely functions of temperature, include the thermal expansion of the spindle. Position dependent thermal errors are functions of both temperature and axial positions, such as linear displacement accuracy along an axis. In this regard, different model forms are utilized to describe those thermal errors, respectively.

The regression model using a least squares estimation [4] is employed in this paper to describe the thermo-elastic relationship due to its simple structure and better extrapolation when compared with other modeling methods such as artificial neural

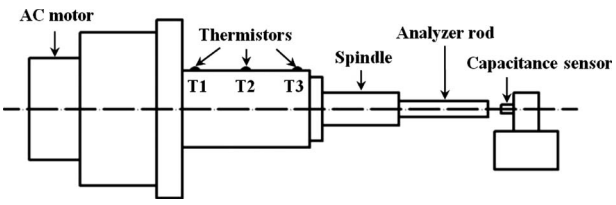

Fig. 8 Experimental setup for spindle thermal expansion

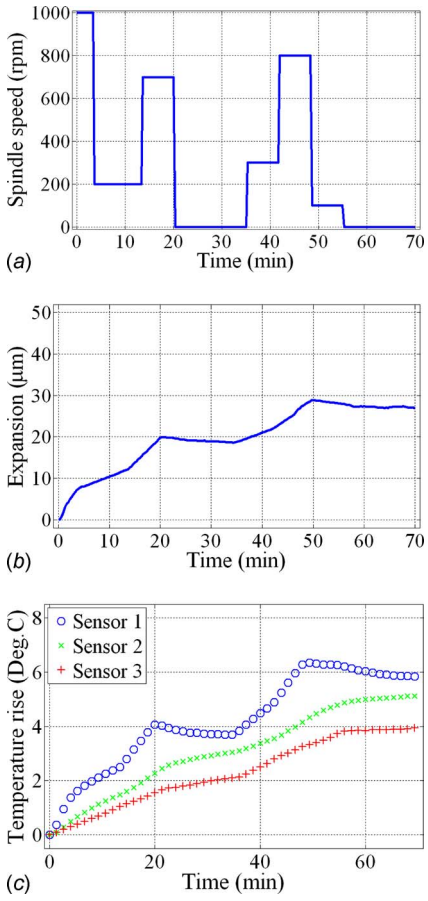

Fig. 9 Experimental results of test 1: (*a*) spindle speed, (*b*) spindle expansion, and (*c*) temperature variations

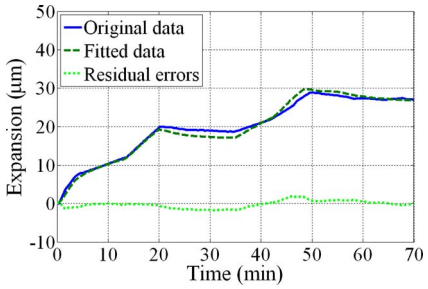

Fig. 10 Measured and modeled results of the spindle experiment

networks.

The formula for position independent thermal errors is in the form of

$$E(t) = \sum_{i=1}^{N} \beta_i T_i(t) \tag{12}$$

where $E(t)$ denotes the thermal errors, t is time, and N is the number of temperature sensors.

The position dependent thermal errors are formulated as

$$E(x,t) = \sum_{i=1}^{N} [\beta_{0i} + \beta_{1i} P(x) + \beta_{2i} P^2(x) + \cdots] T_i(t) \tag{13}$$

where $P(x)$ is the position of the corresponding thermal errors.

In Eqs. (12) and (13), thermal errors, $E(t)$ and $E(x,t)$, are in linear relationship with respect to temperature variation, $T(t)$, which guarantees the extrapolation ability as long as the models are consistent with the data and knowledge of the problem settings. Equations (12) and (13) can be further rearranged in the matrix form of

$$[E] = [T][B] \tag{14}$$

where $[T]=[T_1(t),\ldots,T_N(t)]$ is the temperature matrix, which collects the temperature data captured at different time, and $[B]$ is the coefficient matrix. $[B]$ can be computed by linear least squares estimation

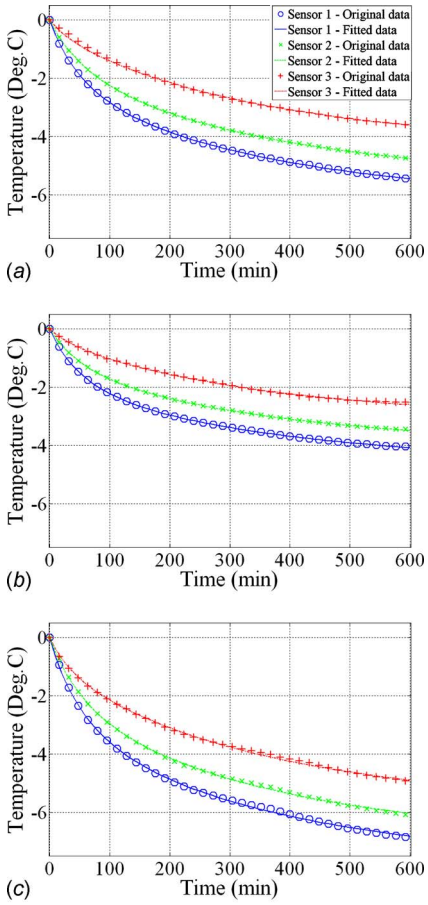

Fig. 12 Temperature variations after each test: (*a*) test 1, (*b*) test 2, and (*c*) test 3

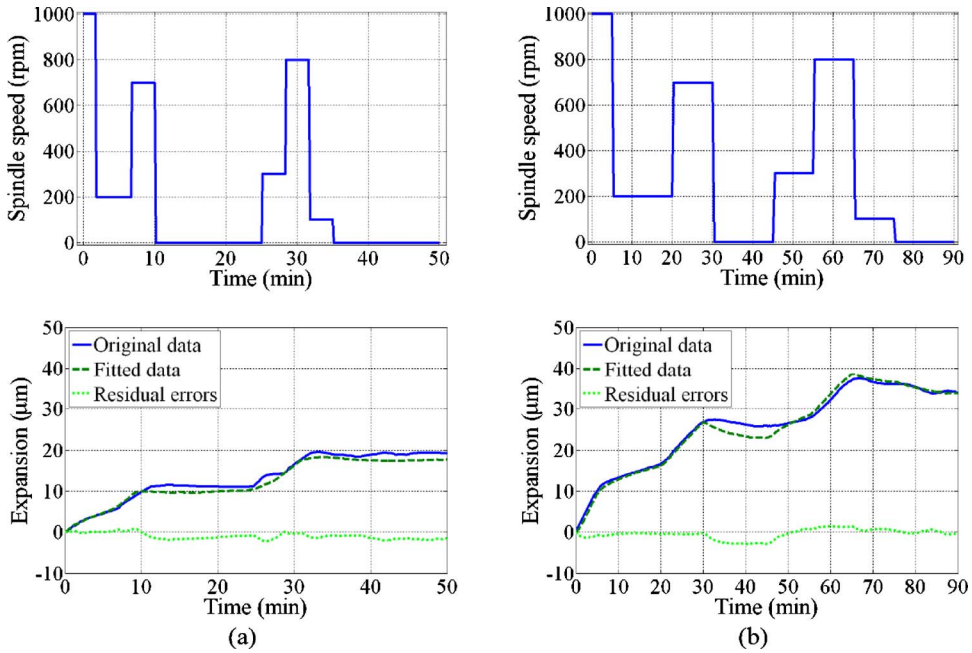

Fig. 11 Spindle speed, measured and predicted thermal errors for robustness verification: (*a*) test 2 and (*b*) test 3

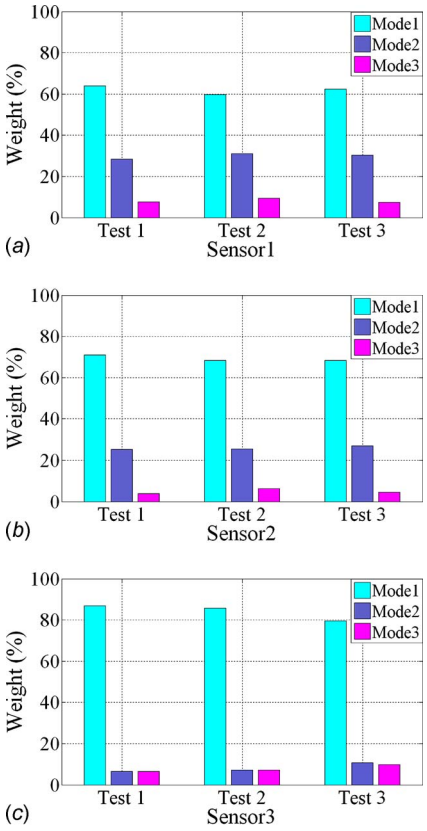

Fig. 13 Weight distributions of the first three thermal modes: (*a*) sensor 1, (*b*) sensor 2, and (*c*) sensor 3

$$[B] = ([T]'[T])^{-1}[T]'[E] \tag{15}$$

Model training is necessary for the estimation of coefficient matrix, $[B]$. During the training, the heat flux inputs are intentionally imposed, while temperature variations and thermal errors are simultaneously collected. In order to justify the robustness of derived thermal error model, linear extrapolation and frequency sensitivity are investigated, respectively. Linear extrapolation is important since it helps reduce the time for the machine characterization and model training. The significance of frequency sensitivity [19] is largely due to the periodicity of machine operations, which causes cyclic thermal loads.

4 Numerical Simulation

In this Section, a machine tool spindle model, as shown in Fig. 1, is used to illustrate the proposed temperature sensor placement

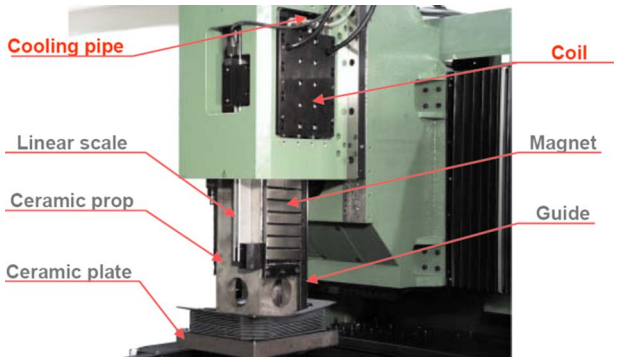

Fig. 14 *Z*-axis structure of an EDM machine (Courtesy of Sodick Inc., Schaumburg, IL)

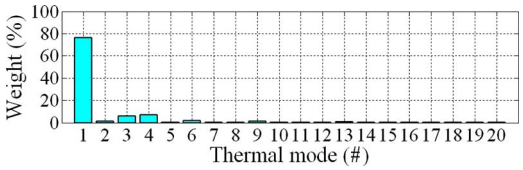

Fig. 15 Weight distribution of thermal modes for the *Z*-axis unit

strategy and thermal error modeling method. There are nine candidate temperature sensor locations along the spindle, indicated by the number above the spindle. The heat input, Q, is assumed to be generated by the spindle motor at the fixed end. Heat exchange exists between the spindle surface and the environment through heat convection. Thermal expansion, ε, occurs at the free end. The geometric parameters and material properties of the spindle model are listed in Table 1.

In order to perform the thermal modal analysis, a finite element model was built. The spindle was divided into 22 elements. By thermal modal analysis, the first four thermal modes with the time constants and the corresponding temperature field distributions are shown in Fig. 2. The magnitudes of the temperature for each mode are normalized. A steplike heat flux was imposed to estimate the modal thermal load and the time constant of each mode. The weight of each mode was then computed according to Eq. (11), and the weight distribution is plotted in Fig. 3. The first three modes contribute more than 90% of the total weights. Temperature sensors are then located for these three modes. According to the proposed temperature sensor placement strategy, one temperature sensor is placed at $x=0.1$ m for thermal modes I and II and another one is at $x=0.5$ m for thermal mode III. For thermal mode I, the sensor is such mounted to approach the heat source as closely as possible since the temperature distribution is relatively uniform. For thermal modes II and III, the sensors are placed around the locations of extreme temperature magnitudes.

The spindle expansion was simulated with the randomly generated heat input shown in Fig. 4. Initially the spindle was at the uniform temperature of 20°C. The temperature variation at locations 1 and 5 and the thermal expansion at the tip of the spindle were collected. Following the procedures in Sec. 3.3.2 a position independent thermal error model was derived to describe the relationship between temperature variation $T(t)$ and thermal expansion $\varepsilon(t)$.

$$\varepsilon(t) = 3.74T_1(t) + 7.36T_5(t) \tag{16}$$

where $T_1(t)$ and $T_5(t)$ represent the temperature variations at locations 1 and 5. The simulation results and modeling results are compared in Fig. 5. Excellent agreement has been achieved between the simulation and modeling results.

In order to examine the robustness of the derived thermal error model, two tests were conducted. In the first test, which spanned 2 h, the first hour of data was used for model training and the remaining hour of data was used for model verification. Results are shown in Fig. 6. The derived thermal error model is reasonably robust in the sense of linear extrapolation, though the modeling results deviate slightly from the simulation results in the second hour. In the second test, heat inputs with different frequencies were generated. The one with a period of 20 min, shown in Fig. 7(*a*), was used to train the model. Two additional heat inputs with periods of 10 min and 40 min, as shown in Figs. 7(*b*) and 7(*c*), respectively, were used for verification. The results suggest that the derived thermal error model is still robust, despite the heat input frequency variations with either higher or lower frequencies. The above two evaluations of model robustness indicate that the proposed temperature sensor locations have already captured the essence of the thermal deformation process.

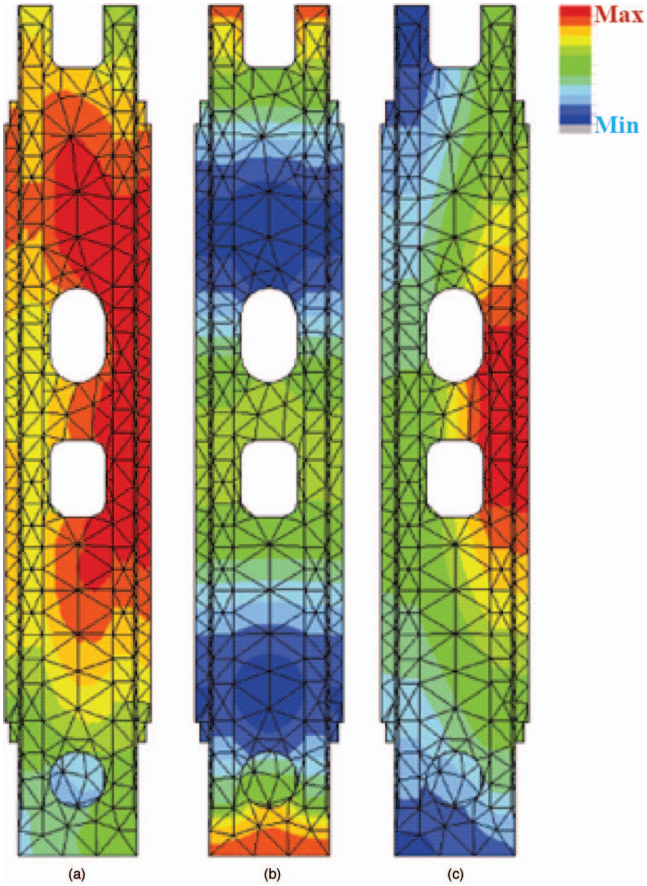

Fig. 16 Temperature field distributions of the dominant thermal modes (front view of the column): (*a*) mode 1, (*b*) mode 3, and (*c*) mode 4

5 Experimental Verification

Two experiments were conducted to validate the proposed thermal error modeling strategy: one on a spindle of a horizontal machining center and the other on the *Z*-axis unit of a die-sinking electrical discharge machining (EDM) machine (Sodick AQ55L). Position independent thermal errors (i.e., thermal expansion of the spindle in the horizontal machining center) and position dependent thermal errors (i.e., linear displacement accuracy along the *Z*-axis of the EDM machine) were analyzed, respectively.

5.1 Position Independent Thermal Error Modeling. Figure 8 shows the experimental setup [13] on the spindle of a horizontal machining center. The spindle is driven by an ac motor. Spindle analyzer was used to measure the thermal expansion of the spindle. Thermistors were employed as thermal sensors in this research. Three temperature sensors were mounted on the spindle housing based on the numerical simulation results in Sec. 4.

One test was carried out at the programed spindle speed, as shown in Fig. 9(*a*). The spindle was warmed up for 20 min, rested for 15 min, and then warmed up for another 20 min, rested for 15 min. The total warm-up time is 40 min. Figures 9(*b*) and 9(*c*) show the measured spindle expansion and temperature variations, respectively. Temperature readings of sensor Nos. 1 and 2 were utilized for the thermal error modeling. The results as well as the residual errors are shown in Fig. 10.

Another two sets of tests were conducted to evaluate the robustness of the thermal error model. The spindle speeds are shown in Fig. 11. The only difference of spindle speeds between the training and verification tests is that the duration of warm-up period, compared with Fig. 9(*a*), is shorten (Fig. 11(*a*)) or elongated (Fig. 11(*b*)) by 50%. The trained model by the first test was used to predict the thermal errors in the two verification tests. The measured and predicted thermal errors are also shown in Fig. 11.

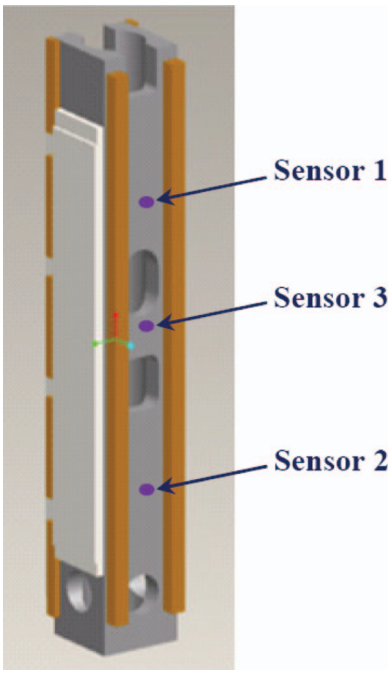

Fig. 17 Temperature sensor placement on the front surface of the *Z*-axis unit

It can be seen from the experimental results that most of the spindle expansion has been described or predicted by the derived model. However, the model does not work well during the cool-down periods. The reason might be that the FEA of the simplified spindle model does not take into account the inner structure of the spindle. The heat source is not merely from the heat generated by the ac motor but from the friction of the spindle bearings as well. It is believed that a more detailed computer-aided design (CAD) model would enhance the FEA results and improve the accuracy of the thermal error model.

To unveil the practical existence of thermal modes, the temperature variations after each test, shown in Fig. 12, were collected at the three locations. These curves were separately fitted by a function of the following form:

$$T(t) = A_1(1 - e^{-t/\tau_1}) + A_2(1 - e^{-t/\tau_2}) + A_3(1 - e^{-t/\tau_3}) \qquad (17)$$

where each term corresponds to one thermal mode, τ_1, τ_2, and τ_3, are the time constants, and A_1, A_2, and A_3 are the weights for the three thermal modes, which are assumed to govern the thermal process. The time constants were estimated to be $\tau_1 = 363.6$ min, $\tau_2 = 61.7$ min, and $\tau_3 = 27.0$ min. The weight distribution of each mode for the three tests is shown in Fig. 13. For each sensor, the weight percentages of three modes under different working conditions are relatively consistent, indicating that the use of weight to distinguish thermal modes is practically meaningful and feasible. Admittedly, the boundary conditions during warm-up and cool-down periods are slightly different, but the fact that several modes dominate the thermal expansion process has been illustrated.

5.2 Position Dependent Thermal Error Modeling. To verify the proposed thermal error modeling strategy for position dependent thermal errors, the *Z*-axis unit of an EDM machine, as shown in Fig. 14, was used. The *Z*-axis is driven by two linear motors with a linear scale as the feedback device. The column is made of alumina ceramics. The total length is 890 mm. The front width is 125 mm, and the side width is 122 mm. The travel range

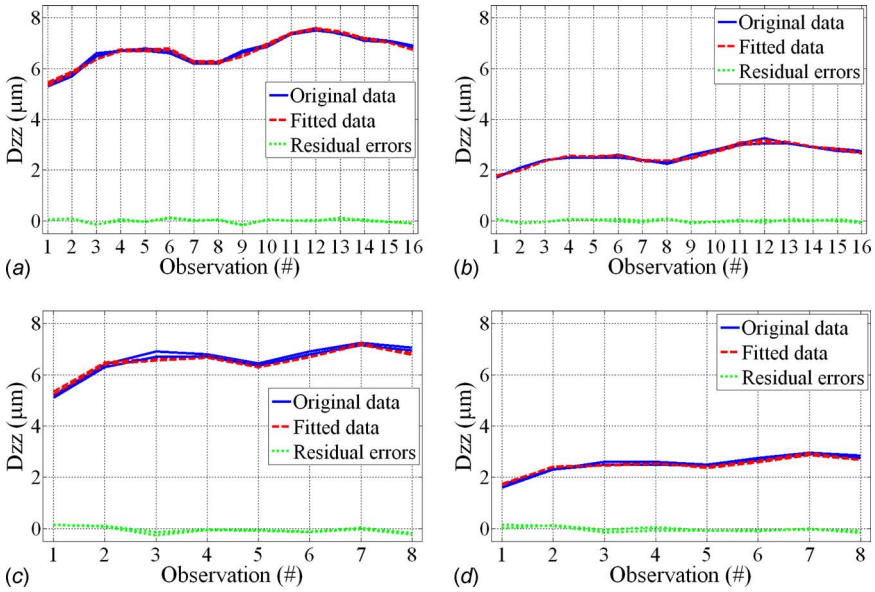

Fig. 18 Comparison of thermal error model training and verification without considering the position effects: (*a*) model training at *Z*=320 mm, (*b*) modeling training at *Z*=160 mm, (*c*) model verification at *Z*=320 mm and (*d*) model verification at *Z* =160 mm

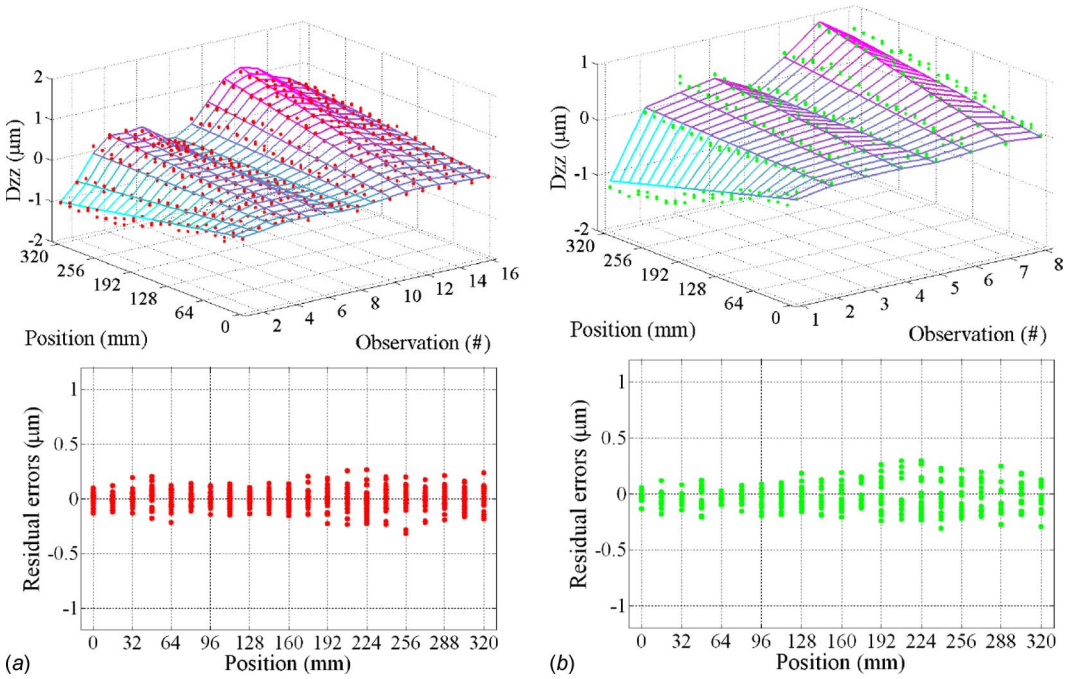

Fig. 19 Linear positioning errors along *Z*-axis model training and verification with residual errors: (*a*) model training and (*b*) model verification

of the *Z*-axis is 320 mm.

Thermal modal analysis was performed to determine the dominant modes. The heat sources are assumed to be from the heat generated by the linear motor coil and the friction of bearings. Heat exchange occurs between the surface of the *Z*-axis column and the environment via heat convection. The weight distribution of thermal modes is shown in Fig. 15. Modes 1, 3, and 4 are the three dominant thermal modes. The corresponding temperature field distributions are shown in Fig. 16. Based on the temperature field distribution of those dominant modes, three temperature sensors were mounted in the front surface of the *Z*-axis column and the locations are illustrated in Fig. 17.

To derive the thermal error model, the *Z*-axis unit was warmed up by continuous movement. The positioning errors along the *Z*-axis, *Dzz*, were measured by using a laser interferometer. The zero position of the *Z*-axis is assumed to be constant throughout the test. Temperature was collected by the mounted temperature sensors during the test. A total of 24 sets of positioning accuracy data was also collected. These 24 sets of data was divided into two groups; one group of 16 sets for model training and the remaining 8 sets for model verification.

The thermal errors at two positions, the far end, $Z=320$ mm, and the middle of the Z-axis, $Z=160$ mm, were first investigated. Two separate position independent thermal error models were derived without taking into account the position factors. The model training and verification results are shown in Fig. 18.

After considering the interactive influence of both temperature and position, a position dependent thermal error model according to Eq. (13) was then derived for the linear displacement accuracy along the Z-axis.

$$E(z,t) = [0.486 - 0.306T_1(t) - 0.081T_2(t) - 2.420T_3(t)] + [0.014P(z) - 0.002P(z)T_1(t) - 0.008P(z)T_2(t) - 0.100P(z)T_3(t)] \quad (18)$$

where $T_1(t)$, $T_2(t)$, and $T_3(t)$ are the temperature readings and $P(z)$ represents the nominal position along the Z-axis as indicated by the EDM machine. The coefficients in Eq. (18) were estimated by using linear least squares method based on the 16 sets of training data. The modeling results and residual errors are shown in Fig. 19. In the model training and verification plots, the dots and the surface denote the measured and modeled thermal errors, respectively. It can be seen from the plots of the residual errors that the linear positioning errors are reduced to $-0.5-0.5$ μm range.

Generally speaking, the proposed thermal error modeling strategy shows significant improvement in modeling both position independent and position dependent thermal errors.

6 Conclusions

In this paper, a robust thermal error modeling strategy through the thermal mode concept was presented. Finite element analysis was utilized to determine the time constant, weight, and temperature field distribution of each thermal mode. Temperature sensors were then allocated to capture the dominant thermal modes of the heat transfer process. By doing this, the essence of the thermoelastic relationship is acquired. Linear regression models were employed to describe both position independent and position dependent thermal errors. Numerical simulation and experiments utilizing a spindle and an axis unit were conducted to reveal the existence of thermal modes and the feasibility of the modeling method. The effectiveness and robustness were also demonstrated in terms of linear extrapolation and frequency sensitivity.

The approach described above relates the theoretical thermal modal analysis framework with the conventional empirical thermal error modeling methods, practically facilitating thermal error compensation techniques. In addition, it provides an efficient and cost-effective temperature sensor placement scheme. A significant amount of time and effort could be saved during the machine tool thermal error model training process by utilizing this methodology. Finally, the accuracy of the derived models could be further enhanced by including additional significant thermal modes.

Acknowledgment

This research is sponsored by the NIST Advanced Technology Program and the POM Group Inc. at Auburn Hills, Michigan.

References

[1] Bryan, J. B., 1990, "International Status of Thermal Error Research (1990)," CIRP Ann., **39**(2), pp. 645–656.
[2] Donmez, M. A., Blomquist, D. S., Hocken, R. J., Liu, C. R., and Barash, M. M., 1986, "A General Methodology for Machine Tool Accuracy Enhancement by Error Compensation," Precis. Eng., **8**(4), pp. 187–196.
[3] Balsamo, A., Marques, D., and Sartori, S., 1990, "A Method for Thermal Deformation Corrections of CMMs," CIRP Ann., **39**(1), pp. 557–560.
[4] Chen, J. S., Yuan, J., Ni, J., and Wu, S. M., 1993, "Real-Time Compensation for Time-Variant Volumetric Error on a Machining Center," ASME J. Eng. Ind., **115**(4), pp. 472–479.
[5] Mou, J., Donmez, M. A., and Cetinkunt, S., 1995, "An Adaptive Error Correction Method Using Feature-Based Analysis Techniques for Machine Performance Improvement. Part I: Theory Derivation," ASME J. Eng. Ind., **117**(4), pp. 584–590.
[6] Mou, J., Donmez, M. A., and Cetinkunt, S., 1995, "An Adaptive Error Correction Method Using Feature-Based Analysis Techniques for Machine Performance Improvement. Part II: Experimental Verification," ASME J. Eng. Ind., **117**(4), pp. 591–600.
[7] Ni, J., 1997, "CNC Machine Accuracy Enhancement through Real-Time Error Compensation," ASME J. Manuf. Sci. Eng., **119**(4B), pp. 717–725.
[8] Chen, J. S., 1996, "A Study of Thermally Induced Machine Tool Errors in Real Cutting Conditions," Int. J. Mach. Tools Manuf., **36**(12), pp. 1401–1411.
[9] Yang, S., Yuan, J., and Ni, J., 1996, "The Improvement of Thermal Error Modeling and Compensation on Machine Tools by Neural Network," Int. J. Mach. Tools Manuf., **36**(4), pp. 527–537.
[10] Srinivasa, N., and Ziegert, J. C., 1997, "Prediction of Thermally Induced Time-Variant Machine Tool Error Maps Using a Fuzzy ARTMAP Neural Network," ASME J. Manuf. Sci. Eng., **119**(4A), pp. 623–630.
[11] Mou, J., 1997, "A Method of Using Neural Networks and Inverse Kinematics for Machine Tools Error Estimation and Correction," ASME J. Manuf. Sci. Eng., **119**(2), pp. 247–254.
[12] Wang, K. C., Tseng, P. C., and Lin, K. M., 2006, "Thermal Error Modeling of a Machining Center Using Grey System Theory and Adaptive Network-Based Fuzzy Inference System," JSME Int. J., Ser. C, **49**(4), pp. 1179–1187.
[13] Yang, H., and Ni, J., 2003, "Dynamic Modeling for Machine Tool Thermal Error Compensation," ASME J. Manuf. Sci. Eng., **125**(2), pp. 245–254.
[14] Yang, H., and Ni, J., 2005, "Dynamic Neural Network Modeling for Nonlinear, Nonstationary Machine Tool Thermally Induced Error," Int. J. Mach. Tools Manuf., **45**(4–5), pp. 455–465.
[15] Kurtoglu, A., 1990, "The Accuracy Improvement of Machine Tools," CIRP Ann., **39**(1), pp. 417–419.
[16] Lo, C. H., Yuan, J., and Ni, J., 1999, "Optimal Temperature Variable Selection by Grouping Approach for Thermal Error Modeling and Compensation," Int. J. Mach. Tools Manuf., **39**(9), pp. 1383–1396.
[17] Lee, J. H., and Yang, S. H., 2002, "Statistical Optimization and Assessment of a Thermal Error Model for CNC Machine Tools," Int. J. Mach. Tools Manuf., **42**(1), pp. 147–155.
[18] Lo, C. H., 1994, "Real-Time Error Compensation on Machine Tools Through Optimal Thermal Error Modeling," Ph.D. thesis, the University of Michigan, Ann Arbor, MI.
[19] Ma, Y., Yuan, J., and Ni, J., 1999, "A Strategy for the Sensor Placement Optimization for Machine Thermal Error Compensation," American Society of Mechanical Engineers, Manufacturing Engineering Division, Atlanta, GA, Vol. 10, pp. 629–637.
[20] Ma, Y., 2001, "Sensor Placement Optimization for Thermal Error Compensation on Machine Tools," Ph.D. thesis University of Michigan, Ann Arbor, MI.
[21] Shah, P. C., and Udwadia, F. E., 1978, "A Methodology for Optimal Sensor Location for Identification of Dynamic System," ASME J. Appl. Mech., **45**(1), pp. 188–196.
[22] Juang, J. N., and Pappa, R. S., 1985, "Eigensystem Realization Algorithm for Modal Parameter Identification and Model Reduction," J. Guid. Control Dyn., **8**(5), pp. 620–627.
[23] Salama, M., Rose, T., and Garba, J., 1987, "Optimal Placement of Excitations and Sensors for Verification of Large Dynamical Systems," *Proceedings of the 28th Structures, Structural Dynamics, and Materials Conference*, Monterey, CA, April 6–8, pp. 1024–1031.
[24] Kammer, D. C., 1991, "Sensor Placement for On-Orbit Modal Identification and Correlation of Large Space Structures," J. Guid. Control Dyn., **14**(2), pp. 251–259.
[25] Moriwaki, T., 1988, "Thermal Deformation and Its Online Compensation of Hydrostatically Supported Precision Spindle," CIRP Ann., **37**(1), pp. 283–286.
[26] Jedrzejewski, I., Kaczmarek, J., Kowal, Z., and Winiarski, Z., 1990, "Numerical Optimization of Thermal Behavior of Machine Tools," CIRP Ann., **39**(1), pp. 109–112.
[27] Attia, M. H., and Fraser, S., 1999, "A Generalized Modeling Methodology for Optimized Real-Time Compensation of Thermal Deformation of Machine Tools and CMM Structures," Int. J. Mach. Tools Manuf., **39**(6), pp. 1001–1016.
[28] Fraser, S., Attia, M. H., and Osman, M. O. M., 2004, "Control-Oriented Modeling of Thermal Deformation of Machine Tools Based on Inverse Solution of Time-Variant Thermal Loads with Delayed Response," ASME J. Manuf. Sci. Eng., **126**(2), pp. 286–296.
[29] Coutinho, A. L. G. A., Landau, L., Wrobel, L. C., and Ebecken, F. F., 1989, "Modal Solution of Transient Heat Conduction Utilizing Lanczos Algorithm," Int. J. Numer. Methods Eng., **28**(1), pp. 13–25.
[30] Dos Santos, F. C., Coutinho, A. L. G. A., and Landau, L., 1990, "New Load Dependent Methods for Modal Solution of Transient Heat Conduction," *Proceedings of the International Conference on Advanced Computational Methods in Heat Transfer*, Southampton, UK, July 17–19, Vol. 1, pp. 51–59.
[31] Matsuo, M., Yasui, T., Inamura, T., and Matsumura, M., 1986, "High-Speed Test of Thermal Effects for a Machine-Tool Structure Based on Modal Analysis," Precis. Eng., **8**(2), pp. 72–78.
[32] Weck, M., Mckeown, P., Bonse, R., and Herbst, U., 1995, "Reduction and Compensation of Thermal Errors in Machine Tools," CIRP Ann., **44**(2), pp. 589–598.
[33] Ahn, J. Y., and Chung, S. C., 2004, "Real-Time Estimation of the Temperature Distribution and Expansion of a Ball Screw System Using an Observer," Proc. Inst. Mech. Eng., Part B, **218**(12), pp. 1667–1681.